Tunnelling and Underground Space Technology 132 (2023) 104856

Contents lists available at ScienceDirect

Tunnelling and Underground Space Technology incorporating Trenchless Technology Research

journal homepage: www.elsevier.com/locate/tust

An investigation of airflow distributions with booster fan for a large opening mine through field study and CFD modeling

Nathan Gendrue [a], Shimin Liu [a,*], Sekhar Bhattacharyya [a], Ronald Clister [b]

[a] Department of Energy and Mineral Engineering, G[3] Center and Energy Institute, The Pennsylvania State University, University Park, PA 16802, USA
[b] Senior Mine Engineer – Western PA, Connellsville, PA 15425, USA

ARTICLE INFO

Keywords:
Metal/nonmetal mine ventilation
Large opening mine
CFD
Mine ventilation
Booster fan
Airflow distribution

ABSTRACT

In this study, we conducted a field survey for the large opening mine with the survey data serving as the numerical modeling inputs to investigate the booster fan airflow distribution using a computational fluid dynamics (CFD) model. A CFD model was created with a booster fan inside the model domain, the airflow distribution patterns around the booster fan were then examined to gain insights on the booster fans impact on the air distribution in the dedicated mining section. Based on the modeling results, the booster fan is an effective ventilation control for airflow direction in large opening mine and the booster fan placement can significantly influence the effectiveness of face pollutants' removal through airflow recirculation. The fan can boost air velocity to create the multi-pillar scale airflow recirculation to dilute the extraction heading pollutants. Furthermore, the typical continuous traverse done by many mine operators, which only covering part of the entire cross section, may be inadequate around booster fans with errors ranging from 35% to 210%. The airflow calculated at the entry adjacent to the booster fan was 25% that of the fan setting with the subsequent entries exchange diminishing by ~65.2% per entry indicating streamlining of airflow in the booster fan entry. While the geometry of the mine will play a significant role in determining the airflow distributions this study lays the groundwork for future studies on booster fan placement optimization and effectiveness for face ventilation.

1. Introduction

The dilutions of hazardous gasses and dusts are essential for mine ventilation systems having implications for both miners' health and overall mine operation safety. When stricter regulations on diesel particulate matter (DPM) were imposed in 2002 from 400 μg/m^3 and finalized in 2008 to 160 Total Carbon (TC) μg/m^3 for underground metal/nonmetal mines, many metal/nonmetal large opening mine operators (entries > 1000ft^2) followed the recommendations of NIOSH publications at the time and implemented propeller fans instead of jet fans for their mine ventilation systems (Grau III et al., 2006, Grau III and Krog, 2009; Grau III et al., 2002, 2004, 2006). The large diameter propeller fans can deliver a high airflow volume to effectively flush out pollutants with the tradeoff of producing little fan pressure. These fans helped meet the objective for the new lower DPM standards, however, questions still remain about the recirculation and streamlined effects in large opening mine environments.

In most underground mines, ventilation controls, including curtains, stoppings, and booster fans, are designed with an intension for their mobility to achieve the best ventilation as mining progresses. Specially, it is critical to adjust these auxiliary ventilation control at the vicinity of active production regions for quickly dilute the pollutants near their sources. However, large opening underground mines are unique due to the negligible airway resistance attributed from the oversized opening dimensions. This allows for huge amounts of air to easily traverse a given airway with the minimum resistance. This leads to a potential engineering challenge to direct airflow in a complex ventilation network. Creating and maintaining these inherently temporary ventilation controls is a multidisciplinary engineering task. The effective ventilation system should consider factors including ventilation economics (operating and capital costs), mine operation, blasting pressures, efficiency, and maintenance over its lifespan.

In large opening mines, booster fans are often used as a ventilation control to enhance or maintain adequate airflow in regions/zones of the mine that are required for air direction or air dilution. In large opening mines booster fans are either vane-axial fans or propeller fans that are placed inside the entry to boost pressure/airflow in the region and direct airflow in the desired direction (Grau III et al., 2002). Compared with

* Corresponding author.
E-mail address: szl3@psu.edu (S. Liu).

https://doi.org/10.1016/j.tust.2022.104856
Received 6 April 2022; Received in revised form 30 August 2022; Accepted 11 November 2022
Available online 25 November 2022

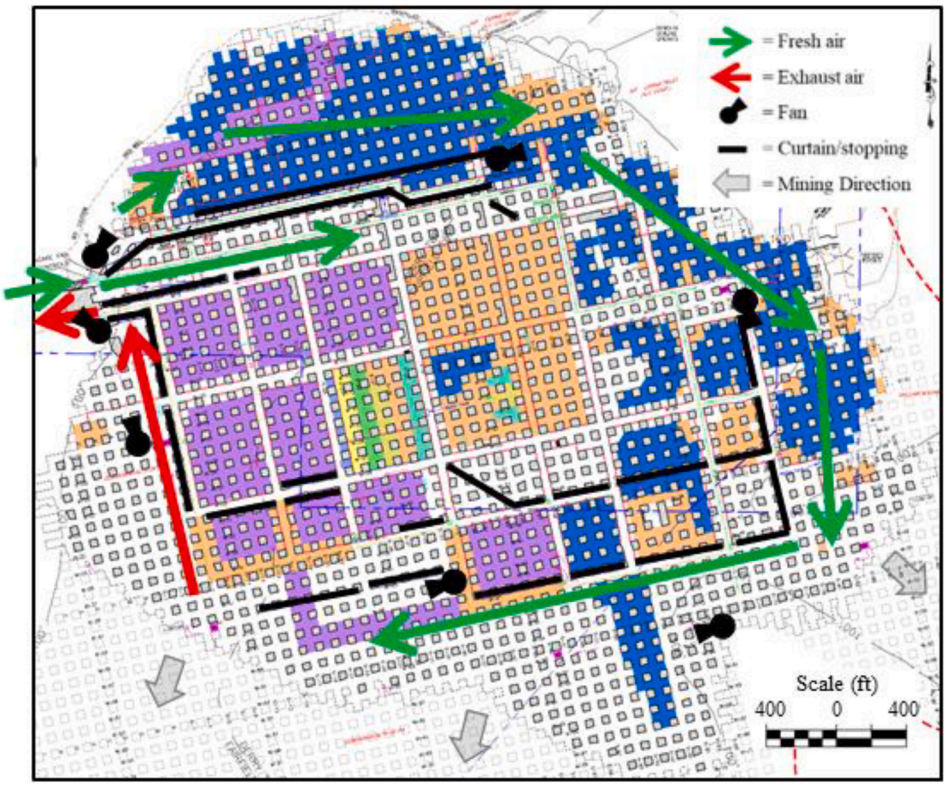

Fig. 1. Mine map of the partner underground large opening mine, ventilation controls are emphasized, map shading indicates benching levels.

small opening mines, the booster fan(s) can be quickly set up and the maintenance cost is low in large opening mines. However, it is known that the improperly positioned booster fan(s) can create a high velocity air stream creating short circuits at adjacent entries which are away from the pollutant sources. Furthermore, booster fan(s) can also redistribute the pressure pattern such that recirculation is possible and/or air leakage can be minimized. For the large opening mine application, booster fan(s) therefore can provide desirable overall airflow directing control through pressure optimization if the fan was placed at an optimal location.

Previous investigations demonstrated the position of booster fan(s) at underground airways is "the most important aspect", (Grau III et al., 2002) for fan performance and overall ventilation effectiveness. To date, the positioning of booster fans in large opening mines is largely empirical based. Since the positioning of booster fan(s) is crucially important for ventilation system, the systematic analysis of booster fan placement and optimization should be rigorously studied. It is challenging to theoretically study the large opening mine booster placement and optimization due to three primary reasons. Firstly, the industry does not routinely conduct mine-scale ventilation survey which results in the lack of open-source data for ventilation modeling. Secondly, the conventional ventilation network models are not well suited for large opening mine environments because the errors associated with P-Q surveys and the reliance on pressure-based iteration methods. The room and pillar mine geometries further complicate the networks with remote areas in the networks having airflow values differing by magnitudes. Thirdly, the complex and unsteady airflow is common due to the local operation and the seasonal atmospheric variations. Thus, other numerical methods should be considered to employed for the large opening ventilation planning and optimization.

Numerical simulations such as CFD have gained immense popularity among researchers in recent years due to its low costs and balance between accuracy and computing power. The mine-scale booster fan effectiveness assessment using computational fluid dynamics (CFD) is the thrust of this study. We conducted a ventilation survey at one of our partner mines. The survey data was used to create a CFD model of a section of an underground large opening stone mine. Booster fan effectiveness was assessed in terms of airflow in adjacent entryways and crosscuts. We then provided a detailed discussion on the booster fan effectiveness. The study provides a theoretical basis for booster fan placement strategy which will lay the foundation for further studies on booster fan optimization both in terms of its local effect and overall ventilation system optimization.

2. Background and literature review

The National institute for Occupational Safety and Health (NIOSH) conducted numerous studies on large opening mine ventilation design and standardization in the early 2000′s. Three major factors were identified and discussed specifically large opening mine ventilation systems: overall design of the system, fan selection, and ventilation controls (Grau III et al., 2002; Grau III et al., 2004a). The use of high-volume low-pressure propellor fans rather than jet fans in large opening mines was recommended due to the low ventilation resistance in large opening mines. Large opening mine operators were also keen to adopt such guidance due to the stricter regulations for diesel particulate matter that were finalized in 2008 per CFR 57.5060 (Code of Federal Regulations, 2018).

Krog et al. (Krog et al., 2004) introduced and discussed terminologies to classify different ventilation schemes for large opening mines such as split, perimeter and unit ventilation systems. The key difference between split and perimeter ventilation systems is that, in split ventilation scheme, the curtain/stopping line is constructed parallel to the mining direction while in perimeter ventilation the line is constructed perpendicular to the mining direction. These two schemes offer significantly different ventilation airflow systems that are fundamentally different. In the perimeter scheme, the older portions of the mine are bypassed in order to increase ventilation effectiveness in active mining regions. These studies offered the experience-based ventilation guidance for large opening mines and these studies were based on field measurements

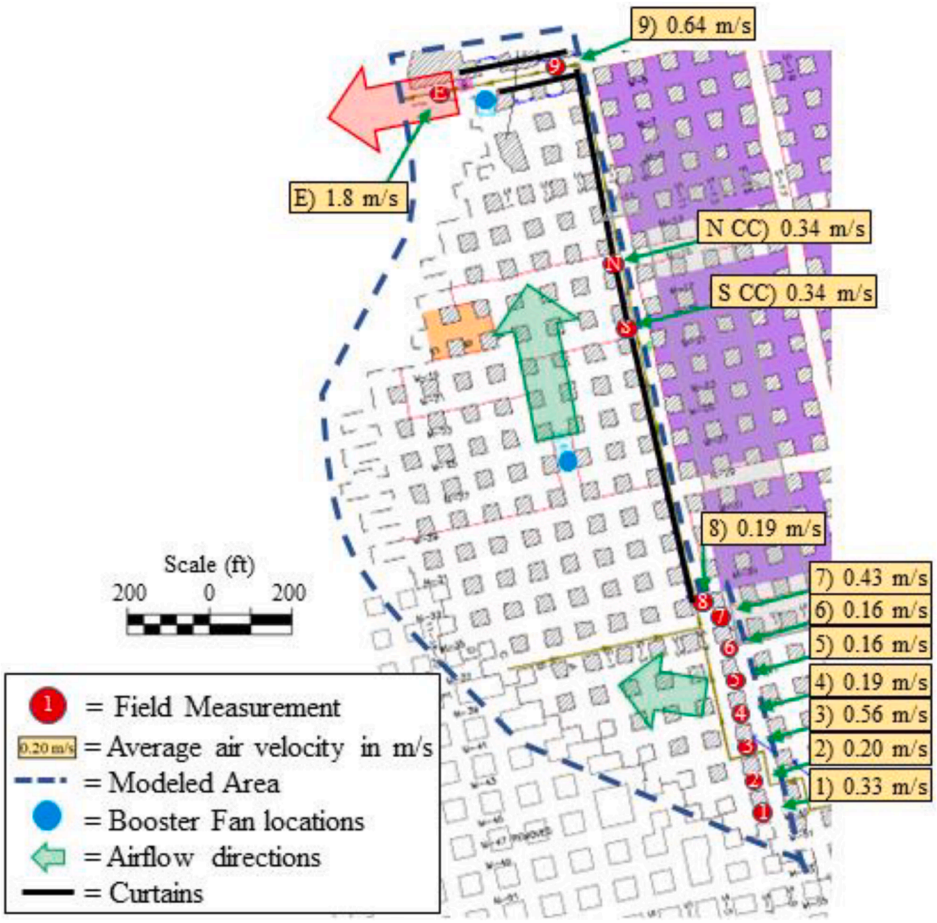

Fig. 2. Section of the mine used for the CFD simulation; 12 locations were measured and marked as red circles 11 were used as inlets with 1 defined as the outlet for the CFD model, the airflow pattern is shown as green arrows, the exhaust portal is shown by the red arrow. (For interpretation of the references to color in this figure legend, the reader is referred to the web version of this article.)

and surveys. However, the fundamental driving forces of the large opening mine ventilation system is the combination of natural ventilation pressure and the mechanical fans. It remains unclear the relative roles of natural ventilation pressure and fan air movements at different scales of temporal (diurnal and seasonal) and spatial (meters to kilometers) dimensions. Thus, mechanism-based modeling of large opening ventilation system is essential to understand the driving forces of the system and provides the baseline information of ventilation planning and optimization.

CFD is known for its versatility of modeling complex fluid dynamic systems, and it has become a powerful tool for ventilation studies. Xu et al. (Xu et al., 2017) showed that CFD has been widely used in the mining industry for a number of specific engineering problems such as: mine ventilation airflow, spontaneous combustion, mine fires, methane flow and control, gob gas flow, inertization of the gob, dust dispersion and control, and mineral processing studies. Zheng and Tien (Zheng and Tien, 2008) used CFD to simulate a large portion of the mine to determine the effectiveness of a large opening mines' main ventilation airflow system, concluding that even with proper stopping line placements portions of the mine remain poorly ventilated. The author then created new smaller simulations to specifically optimize the auxiliary ventilation in these concerned regions. (Hargreaves and Lowndes, 2007) simulated a continuous miner face with 12 independent model geometries assessing the effectiveness of auxiliary ventilation system at different stages in the mining process. It is apparent that many of these CFD studies either are focused on coal mining, or auxiliary ventilation for metal/nonmetal mines (Aminossadati and Hooman, 2008; Xu et al., 2017). As noted in Grau (Grau III et al., 2002), many common ventilation techniques that are used in small opening mines are not readily adaptable for large opening mines due to the oversized entry and presumably costs. Therefore, many of these CFD studies may not be directly related to a large opening mine application.

Booster fans have become essential for large opening mines and studies on booster fan effectiveness are scares in the literature but there are some noteworthy publications. Dunn et al. (1983) conducted numerous studies on jet fan performance in large cross-sectional airways. Nine booster fan positions were investigated only to conclude that 25% to 50% of the booster fan airflow entered the face area. Recirculation was also discussed and ranged from 40% to 90% of the fan airflow. This recirculation was found around the pillars nearest the booster fans in all cases but was not found around the face areas. Goodman and his co-workers (Goodman et al., 1992) studied four jet fan configurations (only fan, fan + nozzle, fan + injector tube, fan + flow injector) to determine their effectiveness in ventilating deep cuts up to 27.5 m (90 ft). However, only the fan configuration of the fans was investigated and not the positioning. Grau III et al (Grau III et al., 2004b) discussed improving ventilation effectiveness by creating bulkheads around the main fans in large opening mines as well as the importance of properly installed and maintained curtain/stopping lines. Through this case study, they doubled the fresh airflow into the mine while lowering the total horsepower used by all fans by ~ 10%. As noted in Grau III et al. (Grau III et al., 2002) the position of booster fan(s) in the mining section is the most important aspect of fan performance. With such an important factor for booster fan performance only Dunn et al (Dunn et al., 1983) studied how the exact position in the mining section effects the face ventilation. The effect of booster fan placement on face

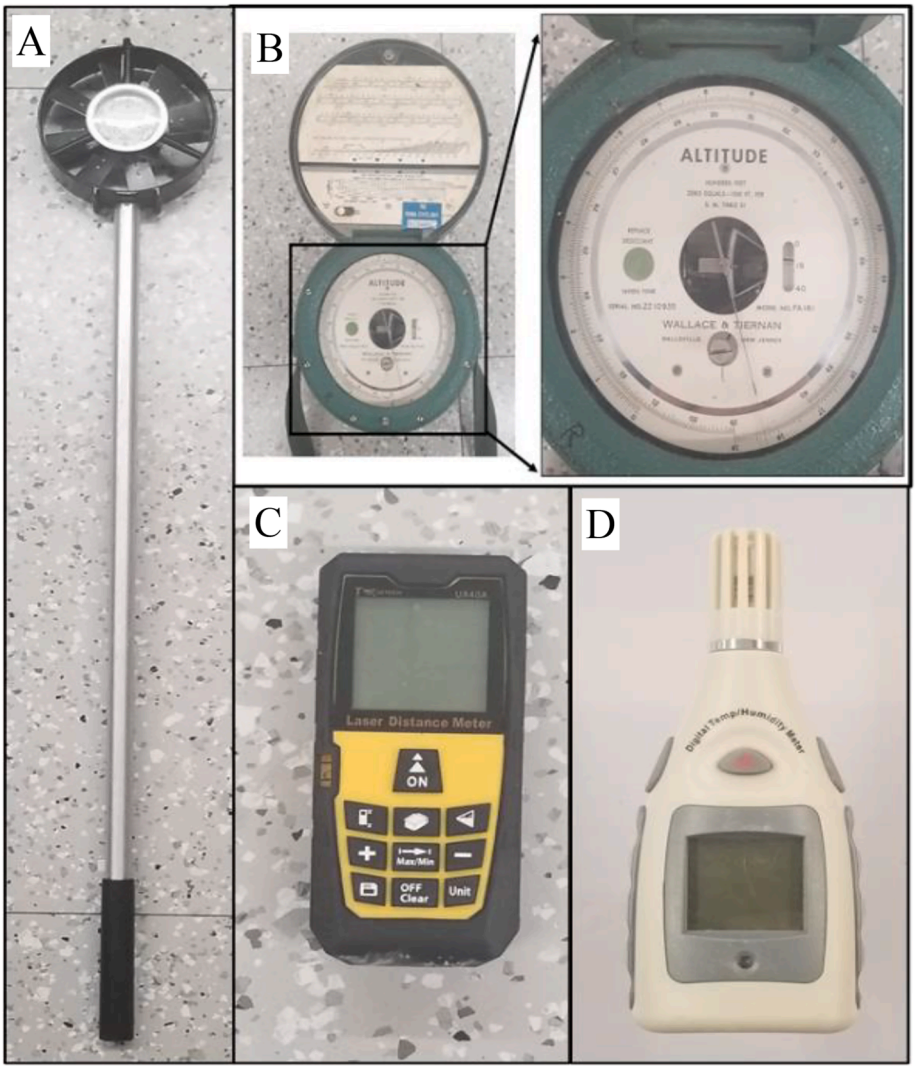

Fig. 3. Instruments used for atmospheric in-mine field investigation a) vane anemometer, b) altimeter, c) digital laser distance measurer, d) relative humidity and temperature sensor.

ventilation needs to be fully and systematically investigated.

While many studies focused on auxiliary ventilation controls, many do not model a fan within the geometry and rather use a boundary condition presumably for simplicity (Chang et al., 2019; Hargreaves and Lowndes, 2007; Parra et al., 2006; Thiruvengadam et al., 2016; Wala et al., 2003; Zhang et al., 2011; Zheng et al., 2017, 2011). Only studies by one research group (Lee and Nguyen, 2015; Nguyen and Lee, 2019; Nguyen et al., 2019) show low-pressure high-volume fans within the model geometry. Their studies, however, focus on optimizing various auxiliary ventilation schemes in a single entry of a large opening mine using pressurization techniques and unducted systems. Using a boundary defined airflow instead of a fan in the geometry is adequate for these typical single entry or duct and curtain type auxiliary controls. Certainly, this CFD scheme is inadequate for modeling large opening room and pillar mines, such as limestone or salt mines, where multiple entries sweep across the working face with little ventilation controls other than a booster fan. In these mines, multiple working faces are mined per shift and the typical auxiliary ventilation systems seen in coal and metal mines are not utilized likely due to their economic impracticality (Grau III et al., 2006). To our best knowledge, no CFD models have been reported overall airflow modeling and optimization where a booster is in the model domain and multiple entries are left open for airflow to traverse across the working faces. Therefore, this study aims to discuss booster fan performance specifically for underground large opening mines.

3. Research method

3.1. Mine description and field survey method

In the spring of 2020, in-mine atmospheric data was monitored, recorded and collected from our partner underground limestone mine in Pennsylvania. The purpose of the in-mine survey was to determine the boundary conditions for the proposed CFD model to quantitatively investigate the booster fan performance and its effectiveness near the working face. The partner large opening underground limestone mine uses a typical perimeter ventilation scheme with their curtain line being approximately 6 openings outby the active mining face. The partner mine uses brattice cloth as their curtains that are 30 ft. and 40 ft. in height and width. The curtains are anchored at the roof to allow the curtain to freely swing to balance the pressure and avoid damage during production blasting. Fig. 1 shows the mine map with the ventilation controls illustrated with the shading of the mine map indicating different levels of benching that has occurred in the regions. An exhaust region of the perimeter scheme was chosen for the CFD modeled region because it has one booster fan in the interior of the geometry, hereby

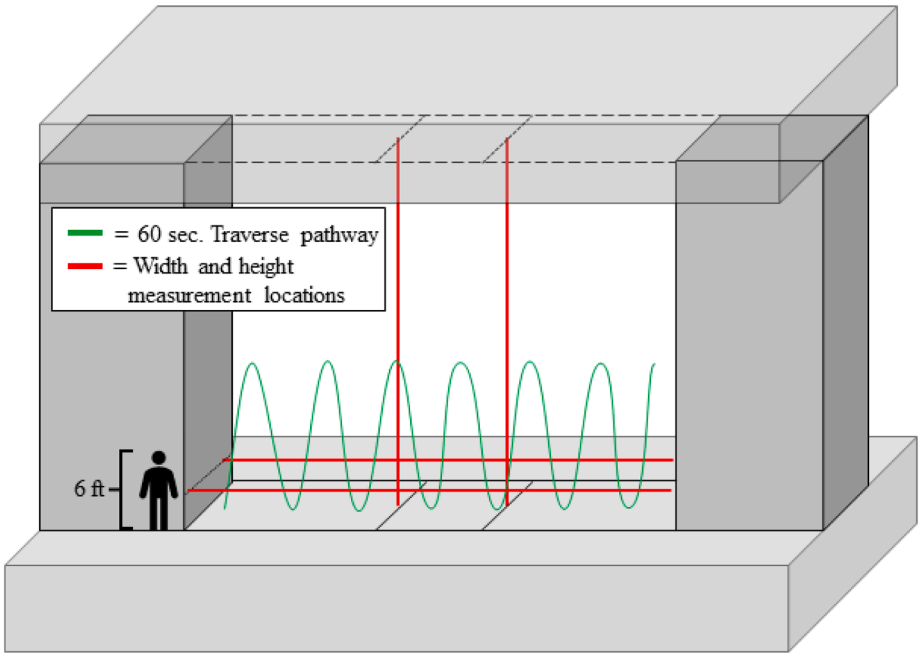

Fig. 4. Locations of the width and height measurements, and 60-second anemometer traverse for the in-mine ventilation survey.

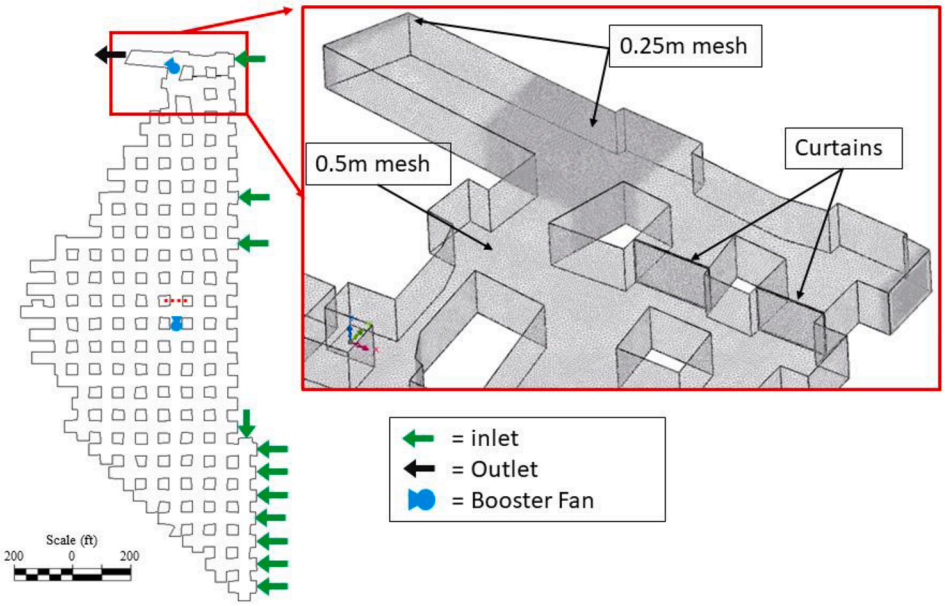

Fig. 5. CFD model geometry in plan-view, the zoomed region of the geometry shows the unstructured meshing with a 0.5 m target element size and the refinement zones with a 0.25 m target element size, the only two curtains within the model geometry are also.

Table 1
Analysis conditions for the CFD simulation.

Model Type	Steady State, RANS - standard k-ε
Fluid	Air - incompressible (1.206 kg/m3)
Gravity	-Z direction
Initial Pressure & Temperature	94 kPa, 17 °C
Inlet conditions	Mass flow defined
Outlet conditions	Pressure defined
Wall condition	rough surface, wall roughness = 0.04 m
Booster fans	Constant Volume flux - (mine defined airflow values)
Convergence criteria	$5*10^{-4}$

labeled interior booster fan (IBF) and one exhausting main fan near the exhaust portal hereby labeled exhaust fan (EF). Fig. 2 shows the section of the mine chosen for the field survey as well as all 12 measurement locations show as red circles. The general airflow pattern is marked by green arrows while the exhaust portal at the top left of the section is marked by the red arrow. During the field mine ventilation survey, the temperature, relative humidity, air velocity, cross sectional area, exact booster fan locations, and barometric pressure were surveyed and collected. Fig. 3 shows the instruments used during the field survey. All altimeter measurements were taken on the floor of the mine with temperature relative humidity reading taken at waist height (approximately 1 m (3 ft.) off the mine floor). The cross-sectional area was measured from the average of two width and height measurements. The two width

Table 2
In-mine ventilation survey data from a section of the underground partner mine.

Location	Variable				
	Velocity (m/s)	Pressure (kPa)	Cross sectional area (m^2) ((±10)	Temperature (°C) (±0.5)	Relative humidity (%)
Inlet 1	0.33	94.6	110	14.5	52
Inlet 2	0.20	94.6	110	14.5	52
Inlet 3	0.56	94.6	110	14.5	52
Inlet 4	0.19	94.6	90	16.0	50
Inlet 5	0.16	94.6	110	16.0	50
Inlet 6	0.16	94.6	110	18.0	49
Inlet 7	0.43	94.7	120	15.0	47
Inlet 8	0.19	94.7	120	15.0	50
South CC (S CC)	0.34	94.7	90	16.0	44
North CC (N CC)	0.34	94.7	100	16.0	44
Inlet 9	0.64	94.7	100	16.0	44
Exhaust Portal (E)	1.8	94.4	110	16.0	35

Table 3
Booster Fan operating conditions and descriptions.

Booster fan	Airflow (m^3/s)	Pressure (kPa)	Description of fan
Inner booster fan	200	0.29	Propeller fan, 74.57 kW, 970 RPM, 3.65 m ø
Exhaust fan	190	0.29	Propeller fan, 74.57 kW , 1185 RPM, 3.65 m ø

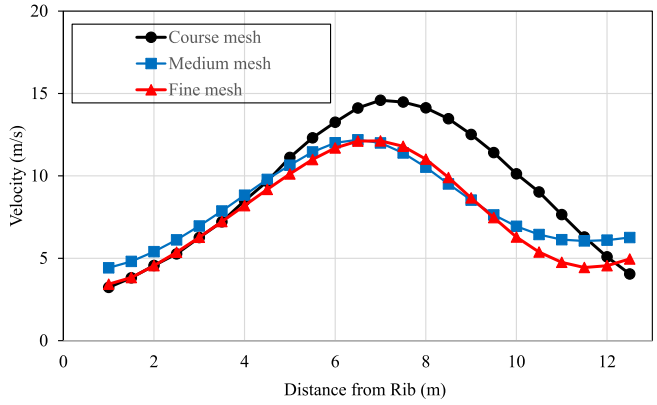

Fig. 6. Velocity profiles for the entry 1 Pillar outby the inner booster fan taken at a height of 2 m.

measurements were also taken approximately 1 m (3 ft.) off the floor and on both ends of the pillar side. The two height measurements were taken approximately 1.5 m (5 ft.) out from the center of the entryway in each direction. Lastly, the 60-second continuous traverse was taken with the anemometer from one corner of the entry to the other. Fig. 4 shows the location of the width and height measurements in red and the pathway for the 60-second traverse in green. The handle of the anemometer is approximately 0.6 m (2 ft.) long which allowed measurements of approximately the bottom ~ 3 m (~9 ft.) of the entry (assuming a 6 ft. man with a 1 ft. arm reach and 2 ft. handle). The total airflow in the full entry was then assumed to have the same average velocity as the continuous traverse. The collected data from the field survey is discussed in **Section 4.1** and can be seen in Table 2.

3.2. CFD model establishment

3.2.1. CFD model geometry

The full-scale CFD model was developed based on the partner limestone mine opening dimensions. The model geometry was established by the mine map with irregular shape pillars for the real case simulation. Since no wall roughness numbers was known, the pillars ribs were modeled as smooth surfaces with wall roughness being accounted for with CFD boundary conditions. The average entry widths and heights are 12.2 m (40 ft.) and 9.1 m (30 ft.) with 24.4 m (80 ft.) pillar centers, respectively. Fig. 2 shows the plan view from the mine map of the region for CFD modeling. The locations of IBF and EF were shown in the blue dots. The measurement locations and velocities for inlet boundary conditions are labeled and shown as red dots. A curtain line with two open cross cuts (labeled N-CC and S-CC) was created by the mine running north to south and is shown as an orange line. For simplicity this curtain line was used as the right edge of the CFD geometry. The northern edge of the geometry is also a curtains line running east to west also shown with an orange line. The mining boundary was used as the edge of the CFD model geometry for the remaining sides. Furthermore, it was assumed that there would be no leakage across any curtain/stopping. Fig. 5 shows a plan view of the CFD geometry with a callout showing the meshing scheme.

3.2.2. Boundary and model conditions

The boundary conditions used in this CFD model were identical to the field collected data from **Section 3.1** and are shown in Table 1, 2, and 3**.** All model inlets (entries) were defined as mass flow inlets with the air velocities concerted to a mass flow rate *via* in mine measured variables (temperature, relative humidity, and pressure). The single outlet (exhausting portal) for the model was defined as a pressure outlet. The booster fans were defined for a specific mass flow based on the information collected from the mine operator as listed in Table 2. The fans were defined as mass flow rather than pressure defined because the industry typically tried to use the high-volume low-pressure propeller fans. Wall roughness was considered in the CFD analysis conditions and assumed to be 0.04 m. The fluid was defined as incompressible air with a constant temperature field. While heat flux from the strata is expected these conditions were made for simplicity and are common among other CFD mining studies (Mishra et al., 2016; Ren et al., 2014; Sun et al., 2018; Wang et al., 2018). The initial temperature and pressures set through the model domain were 17 °C and 94 kPa respectively which was determined by the field survey measurements. Gravity was considered in the Z-direction and the model was solved to a convergence of $5*10^{-4}$ for velocity (X, Y, Z), mass flow, pressure, energy and turbulent energy. The model was run in steady state with a standard k- ε turbulence model. Criteria for mass, momentum, velocity, energy, and turbulent energy were all successfully converged.

3.2.3. Mesh independence study

The airflow distribution and resolution within a CFD modeling is dependent on the mesh sizes. Typically, the finer the mesh is, the higher of accuracy. However, it was also documented that the decreasing the element size of the mesh does not guarantee the better results due to the round off errors (Ren et al., 2014). Therefore, it is essential to perform a mesh independence study to determine the ideal mesh size to optimize computational speed and model accuracy. In this study, three mesh sizes were tested and screened to identify the optimized mesh size. The mesh sizes include coarse-sized, medium-sized, and fine-sized meshes. Fig. 6 shows the velocity profile across an entryway one pillar outby the IBF at a height of 2 m. The location of the velocity profile is shown by the red dotted line in Fig. 5 and consists of 24 points evenly spread across the entry at a height of 1.5-meters above the floor. The velocity profile of the medium and fine meshes match well while the course mesh significantly overestimates the velocity profile on the right side of the entry. Therefore, the medium mesh size was selected for the overall mesh scheme

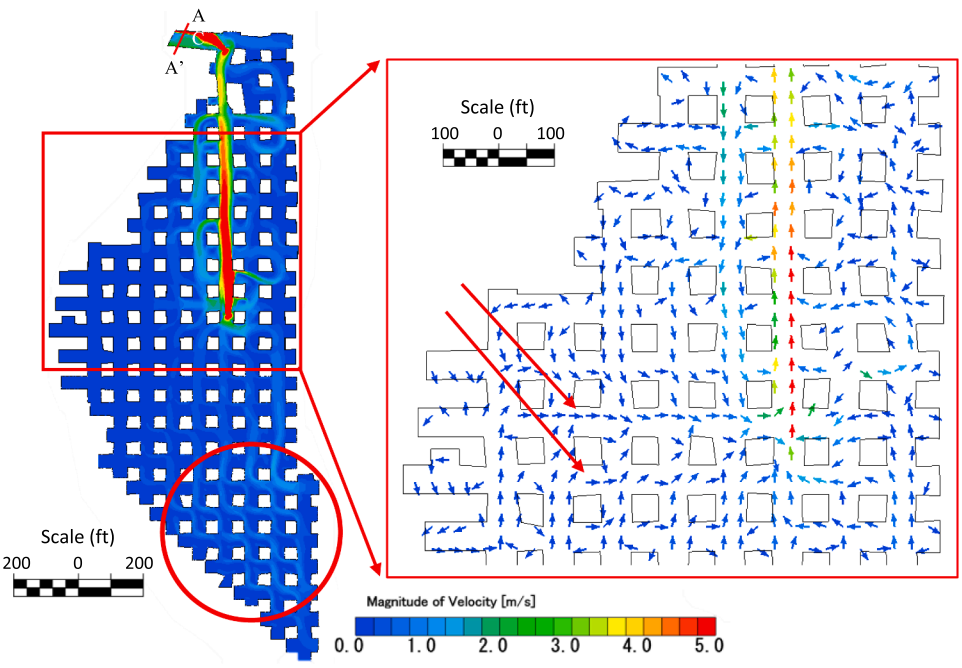

Fig. 7. Velocity contour of model geometry 2 m above the floor, the area around the inner booster fan in enlarged on the right.

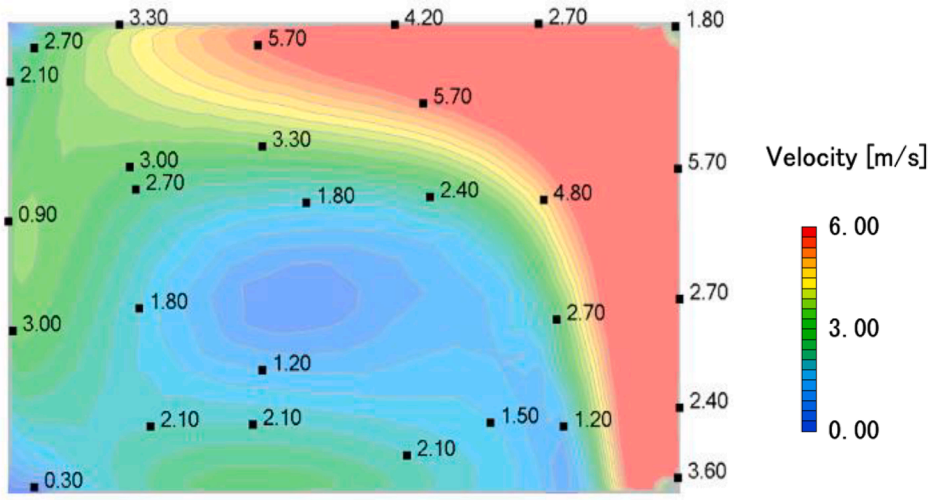

Fig. 8. The velocity profile of the cross sections 5 m inby the exhaust portal.

with the fine mesh only utilized in areas of interest to fully refine the flow such as the boundary conditions and around the booster fans, this scheme resulted in ~ 8.5 million cells. The callout in Fig. 5 shows a portion of the mesh scheme with the medium mesh used throughout the model and the finer mesh highlighted as the denser meshed areas.

3.3. Turbulence model for CFD simulation

There are three major classifications of CFD turbulence models: direct numerical simulations (DNS), large eddy simulation (LES) and Reynolds Averaged Navier-Stokes equations (RANS). DNS and LES provide the most level of details and simulation accuracy; however, the computational requirements needed to simulate these models are immense and typically not undertaken in large modeling projects (Wang et al., 2018). The most widely used model for engineering studies with minimal swirling forces is RANS. Since the model fans were defined by flow this simulation fits well within the scope of RANS models. There are many subdivisions within RANS models: one equation model, two equation model (k-w, k- ε, LRN-LS), multi equation models, and Reynolds stress models (RSM) (Zhai et al., 2007). However, the standard k- ε RANS has been shown to provide an ideal balance between accuracy and computational requirements which is why it was selected for this study (Bakker, 2021; Cai et al., 2018; Kurnia et al., 2014; Mishra et al., 2016; Ren and Balusu, 2005; Tanguturi et al., 2017; Wang et al., 2018; Xu et al., 2017; Yuan et al., 2006).

4. Results and analysis

4.1. Field data

12 measurement locations were surveyed in the mine and the survey data are listed in Table 2. The barometric pressures within the section ranged from 94.6 to 94.75 kPa with only the exhaust portal being lower, near the atmospheric pressure of 94.45 kPa. The air velocity at the

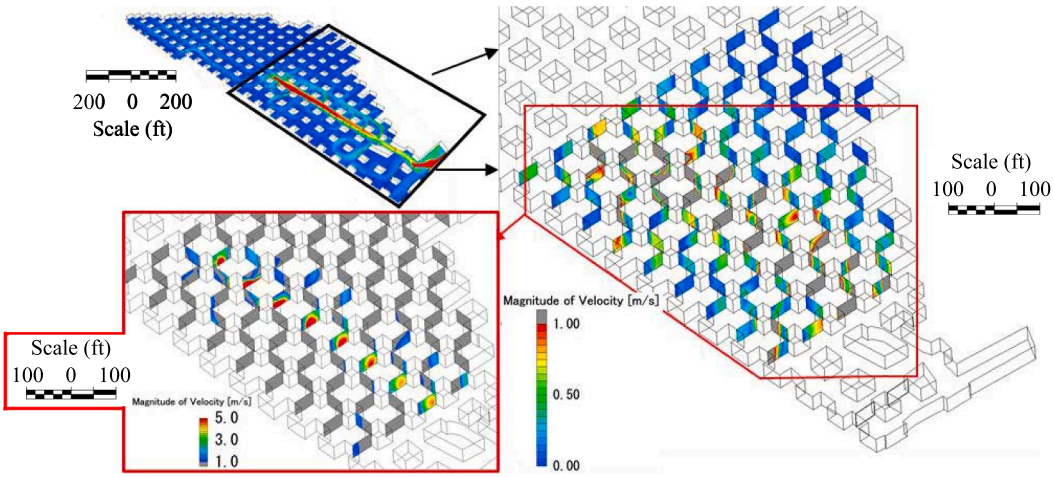

Fig. 9. Velocity contour for entries outby the IBF A) velocity contours from 0 m/s to 1 m/s with velocities greater than 1 m/s shown in grey, B) velocity contours from 1 m/s to 5 m/s with velocities under 1 m/s shown in grey.

exhaust portal was the highest measured airflow at 1.8 m/s with the other 11 entries ranging from 0.16 m/s to 0.64 m/s. Cross sectional areas were variable ranging from 90.3 m^2 to 121.9 m^2. The temperature and relative humidity ranged from 14.5 °C to 17.9 °C and 35% to 52% respectively. The booster fans operating conditions were given by the mine operator and were listed in Table 3, both the booster fans are propeller fans with specifications of ~ 3.65 m (12 feet) and 74.57 kW (100 hp) operating at an RPM of 970 and 1185 respectively. The estimated airflow and pressures given by the operator via the fan curves are also shown.

4.2. CFD modeling results

The CFD model was numerically computed until its convergence of $5*10^{-4}$. The overall velocity contour for the Z plane at 2 m above the floor is shown in Fig. 7 with the area around the inner booster fan highlighted. Fig. 7 also shows velocity vectors scaled to have equal lengths with only the color of the vector showing the absolute magnitude of air velocity. From the results, it is apparent that the inner booster fan significantly influences the localized airflow across the center region of the geometry at 2-meters height above the floor. A highly streamlined air velocity was observed in the booster fan entry with very little airflow elsewhere. The entry immediately to the left of the IBF entry showed airflow opposite of the IBF direction while the entry immediately to the right shows various results with some locations showing airflow reversal and others not. Moving just one entry further in either direction shows a drastic reduction in airflow. These airflow quantities around adjacent entries near the IBF were quantified in the

The EF near the exhaust portal is placed at an angle towards the ribs as determined by the mine survey. From Fig. 7, the highest air velocity is angled toward the northern rib as shown in top-left corner of the geometry. A cross section of was taken from the portal areas as shown by the A-A' line in Fig. 7. Fig. 8 shows this plane 5 m inby and normal to the exhaust portal. This aligns with discussions the author had with the mine operator where they claim to experience high airflow volume along the top portion of the exhaust portal rather than about the whole cross section. When taking in-mine airflow measurements the majority of the airflow in this cross section may not be measured due to the difficulty measuring the upper portion of the cross section. Furthermore, Fig. 9 shows velocity contours in the northern section of the model. XZ and YZ Planes were created in each entry and crosscut to mimic the in mine survey conditions. Each plane was created to be at the center of the pillar line and was extended 7 pillars outby and 1 pillar inby the IBF. Fig. 9A shows the velocities from 0 m/s to 1 m/s with any velocity over 1 m/s shown in grey and Fig. 9B shows the velocities from 1 m/s to 5 m/s with any velocity bellow 1 m/s shown in grey.

4.3. The influence of IBF on airflow around adjacent entries

At the south end of the geometry, in the red circled area in Fig. 7, the airflow is well distributed between all entries flowing from southeast to northwest. This distribution of airflow quickly redistributes once this airflow reaches the IBF. The effect of the IBF fan has a significant influence on its vicinity airflow redistribution, and it should be quantified. Therefore, the airflow between pillars was systemically calculated from the CFD simulation. Fig. 10 shows the locations of the calculated airflow measurement locations in red lines. The entries running north to south are labeled 1_N through 8_N while the entries running east to west are labeled 1_W through 12_W for the simplicity. In entry 1_N, there were 6 velocity averages taken at the center of each pillar, one taken on the pillar separating entries 3_W and 4_W, another at the pillar separating 4_W and 5_W etc. The same method was then used for the entries running east to west. These airflow averages were calculated directly from the simulation file by velocity vector integration multiplied by the calculated cross-sectional area of the cross section. To calculate the average entry velocity, an area weighted vector integration was conducted over the cross section, since the cells in the mesh are not uniform in size and the fluid was treated as incompressible an area weighted average can be used for the estimation. In these calculations, only the normal vector to the XZ or YZ plane contributes to the weighted average.

Table 4 shows the calculated airflow in the eight north–south (N-S) entries from the pillar line inby entry 1_w to the pillar line outby 12_w. The negative airflow values indicate flow in the reverse direction of the IBF and are shaded in blue in the table. There are no negative values inby the IBF in the N-S entries, indicating significant airflow recirculation outby the IBF. Airflow from the IBF's entry (6_N) reaches a maximum of 405.6 m^3/s while the adjacent entries (5_N and 7_N) only reach a maximum of 131.7 m^3/s in the reverse direction. Only one entry other than the fan entry (8_N) observed a positive airflow value outby the IBF. This may be due to a combination of the open cross cuts acting as inlets for the model and the curtain line proving a geometrical boundary on the pillar line adjacent to 8_N. In Table 5, the negative values indicate airflow to the west (towards the face) and are also shaded in blue. Between entries 6_w and 7_w and between pillar lines 5_N-6_N and 6_N to 7_N, there is a cluster of positive values suggest the IBF drawing air from this section of the face area. Airflow patterns inby the IBF (at entry 4_w and outby at entry 10_w or 11_w) indicate the airflow is towards the face area. Thus, we can conclude that the IBF influence over the face areas in entries 1_N and 2_N are limited to two east–west entries inby and outby the location of the IBF. The airflow observed more than two east–west entries inby can be attributed

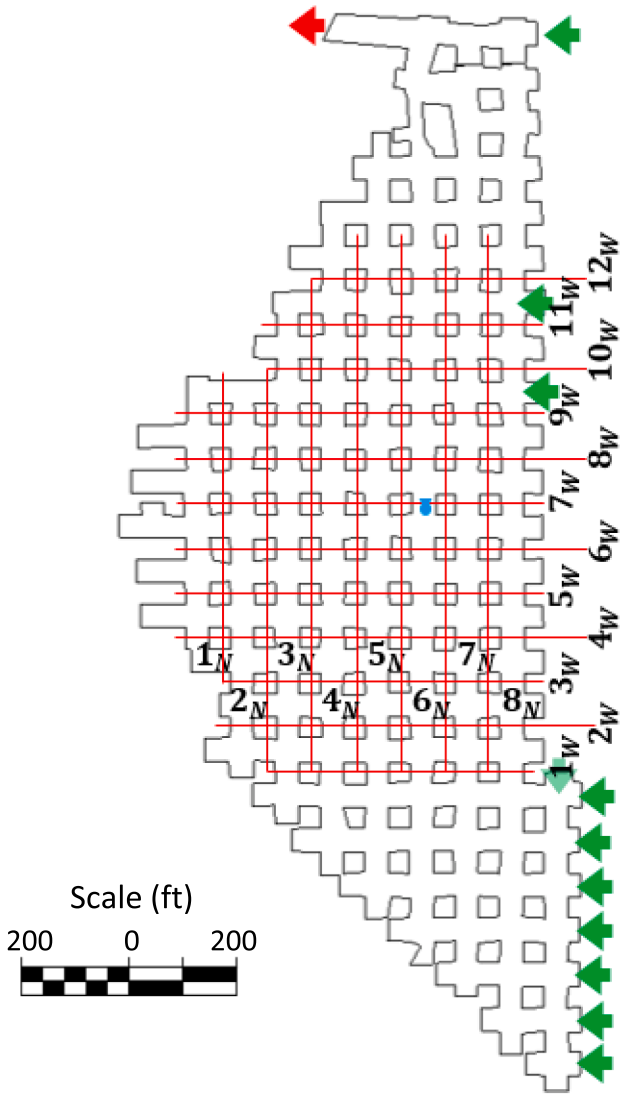

Fig. 10. Location of airflow measurements in the middle section of the model geometry, Northern entries are labeled 1_N-8_N and western entries are labeled 1_W-12_W, the booster fans are labeled as blue fan symbols and green and red arrows are inlets and outlets for the model. (For interpretation of the references to color in this figure legend, the reader is referred to the web version of this article.)

to the air distribution before the IBF while the airflow two east–west entries outby can be attributed to the recirculation caused by the IBF.

These airflow values can be normalized to the airflow setting of the inner booster fan to get a better perspective of the overall airflow. Therefore, the airflow values were scaled by dividing by the inner booster fan setting of 201 m^3/s (425,000 CFM). This allowed us to compare airflows with respect to the IBF, *i.e.* the inner booster fan airflow was scaled to a value of 1 and twice the airflow (850,000 CFM) being 2. Fig. 11A and B shows the scaled values around the IBF from entry 5_W to entry 12_W. The north–south entry airflows are shown in Fig. 11A while the east–west airflow values are shown in Fig. 11B. All scaled values are shown as positive numbers with the arrows showing their respective direction normal to the plane from which the value was calculated. In the entries around the face area in Fig. 11A (1_N and 2_N), the airflow is less than 0.1 times the IBF setting. This suggests there is limited airflow exchange at the face region. Whether it is sufficient for the pollutant dilution, it requires future investigations. Furthermore,

Table 4
Calculated airflow from the CFD simulation file in the N-S direction in m^3/s. The blue shaded numbers indicate negative (reversed) airflow values from that of the IBF flow direction.

N-S entries / E-W cross cuts	1_N (m^3/s)	2_N (m^3/s)	3_N (m^3/s)	4_N (m^3/s)	5_N (m^3/s)	6_N (IBF) (m^3/s)	7_N (m^3/s)	8_N (m^3/s)
12_W-				3	-114	372	19	4
11_W-12_W				-5	-128	406	-15	22
10_W-11_W			-22	-18	-78	405	-33	9
9_W-10_W			-29	-43	-119	442	-21	33
8_W-9_W	-1	-4	-19	-34	-132	377	-15	58
7_W-8_W	1	-0	-12	-23	-68	372	-36	1
6_W-7_W (IBF)	4	4	6	12	38	231	-81	18
5_W-6_W	6	10	15	22	49	62	17	50
4_W-5_W	6	11	16	25	39	40	32	61
3_W-4_W	4	12	20	24	32	35	38	67
2_W-3_W		15	17	20	29	34	48	69
1_W-2_W		10	9	16	32	48	54	62
-1_W			10	27	41	42	54	56

Table 5
Calculated airflow from the CFD simulation file in the E-W direction in m^3/s The blue shaded numbers indicate negative (reversed) airflow values from that of the IBF flow direction.

N-S cross cuts / E-W entries	1_N-2_N (m^3/s)	2_N-3_N (m^3/s)	3_N-4_N (m^3/s)	4_N-5_N (m^3/s)	5_N-6_N (m^3/s)	6_N-7_N (m^3/s)	7_N-8_N (m^3/s)
12_W				-8	-18	16	-17
11_W			-22	-35	11	10	-8
10_W			-6	-32	-72	-36	-23
9_W	-1	-5	5	14	1	-62	-57
8_W	2	3	9	20	84	78	57
7_W	4	10	29	64	170	27	-17
6_W	2	7	16	26	38	-130	-32
5_W	0	2	4	7	-4	-26	-11
4_W	-3	-2	1	1	-7	-11	-5
3_W	-4	-0	-4	-8	-11	-12	-2
2_W		-5	-13	-16	-13	1	6
1_W		-10	-9	1	9	4	4

entries 3_N and 4_N only reach at most 0.2 times the IBF setting. Based on Fig. 11A, the recirculation primarily happens within the two entries away from IBF. We want to point out that the booster-induced recirculation is the key factor for the face pollutants' dilution. Even though the absolute airflow exchange at the face is not large, it may be the leading effect for the sufficient pollutants' removal. In Fig. 11B, the maximum exchange rate between north–south entries is 0.8 and 0.6 times the IBF setting. Both values occur in the cross cuts directly inby and outby the IBF position. Until the pillar line between entries 4_N and 5_N is reached there is only 1 value exceeding 0.1 times the IBF setting. Further indicating the lack of air exchange between the face areas (1_N −4_N) and the IBF entries (5_N through 7_N).

Figs. 12 and 13 shows the calculated airflow values from Table 4 and 5 segregated by the entry in which they were taken. Fig. 12 shows the north–south entries while Fig. 13 shows the east–west entries with the red line on both graphs showing the entry position of the IBF. In Fig. 12 in the 6 entries inby the IBF the airflow is well distributed between 0 m^3/s and 50 m^3/s while the 6 entries outby the IBF show one extremely high airflow value with the remaining entries near or below 0 m^3/s (i.e., flow reversal). Thus, if the airflow measurement is taken in the IBF entry a high airflow value would be obtained but this value is not representative of the section is it supposedly ventilating. In Fig. 13 which shows the east–west entries a steady decrease in airflow exchange can be seen to the left of the red line. In the cross cuts nearest the face (1_N-2_N) the airflow exchange between the north–south entries reaches a maximum of 3.7 m^3/s. The exchange rate does not reach near or above 50 m^3/s (~0.25 times the IBF setting) until the cross cutes between 4_N and 5_N

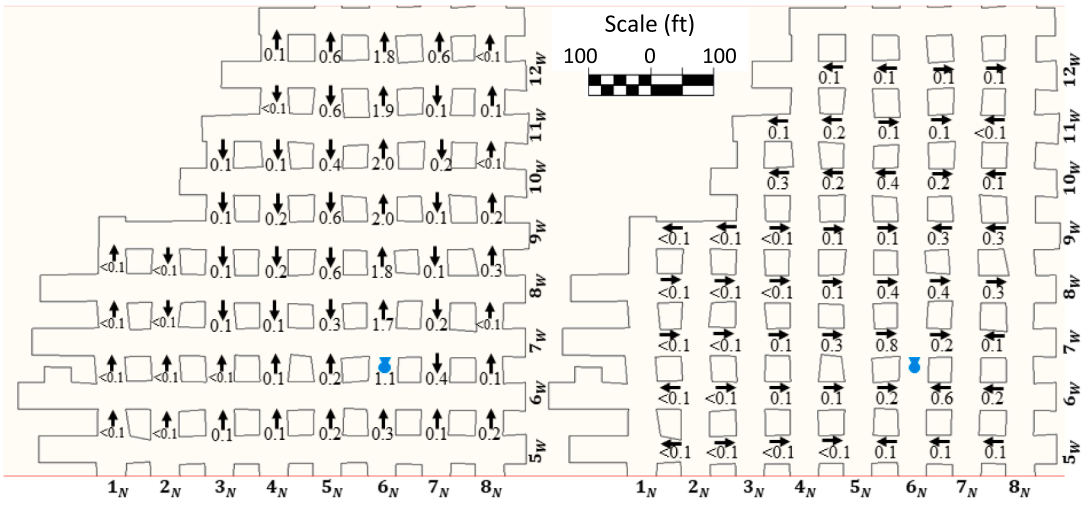

Fig. 11. Calculated area weighted airflows scaled by the inner booster fan airflow settings of 425,000 CFM (201 m^3/s), A) scaled airflows from the north–south entries B) scaled airflows from the east–west entries.

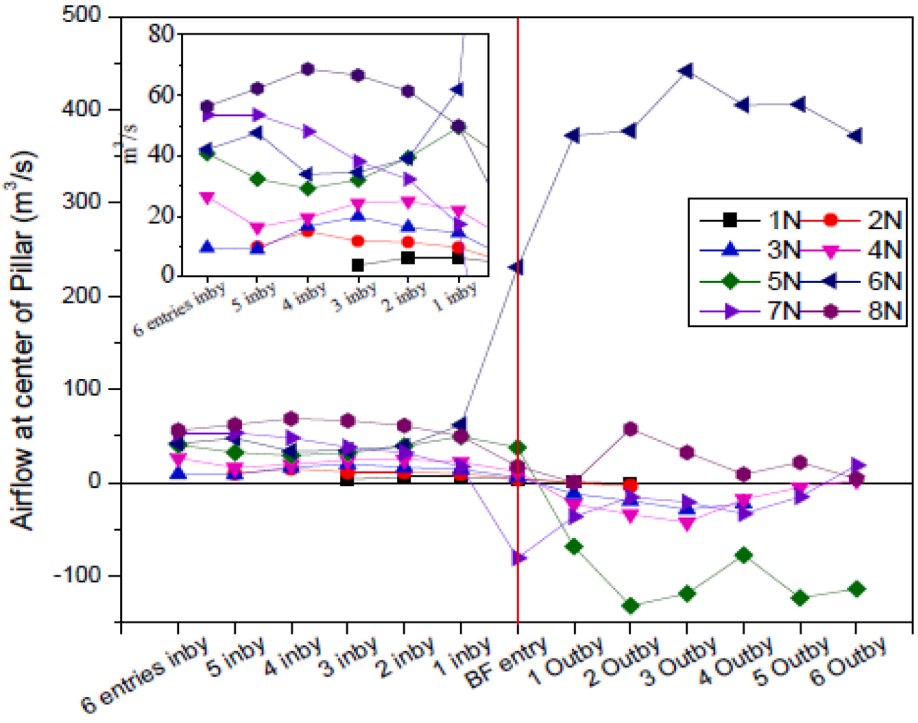

Fig. 12. Calculated entry airflow through the 8 North-South entries (1_N-8_N), Airflow in the booster fan (red line) entry jumps from ~ 50 m^3/s to 300–400 m^3/s while the remaining entries are all below 50 m^3/s with some showing negative airflow values (revered airflow direction). (For interpretation of the references to color in this figure legend, the reader is referred to the web version of this article.)

with the highest airflow in the pillar line between entries 3_N and 4_N calculated at 29.0 m^3/s. This accounts for a 65.2% drop in airflow per entry between entries 4_N and 1_N. Therefore, it can be said the IBF's influence is at minimum 25% of the fan's setting up to two adjacent entries in either direction (6_N to 4_N, or 6_N to 8_N). For the entries further than 2 adjacent from the IBF position a ~ 65% decrease was then calculated from the initial 25% of the IBF setting.

5. Discussion

5.1. Cross sectional velocity profile

Airflow measurements *via* cross sectional area and continuous traverse have long been standard in the mining industry. However, the large opening mine air velocity survey provides a unique challenge because typically over half the entry cannot be easily measured with a mechanical-vane anemometer (McPherson, 1993). Through conversations with many mine operators, it is typical for daily airflow measurements to only measure the bottom half of the entryway and extrapolate the velocity reading to the entire cross section. This practice

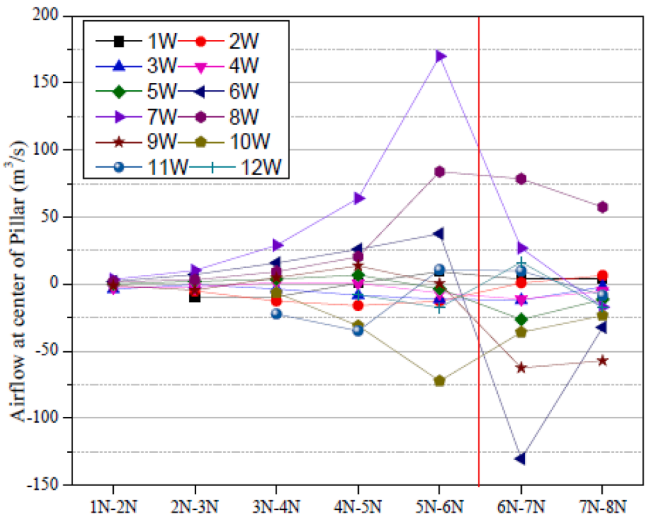

Fig. 13. Calculated airflow through the East-West entries (cross cuts) from 1_W to 12_W, airflow maximizes around the booster fan entry (red line)and gradually diminished in magnitude each entry away ending near zero m^3/s at cross cuts 1_N-2_N. (For interpretation of the references to color in this figure legend, the reader is referred to the web version of this article.)

is much quicker for the operator while also providing the convenience of not requiring large rods which makes the traverse more cumbersome. However, near the booster fans egregious errors can occur if only part of the cross section is measured. Fig. 14A-D shows four cross sections taken throughout the CFD geometry with various levels of accuracy between the total airflow volume and extrapolated airflow volume from only the bottom three meters of the cross section. Fig. 14A shows a cross section 1 pillar outby the IBF while Fig. 14B shows a cross section 4 pillars outby the IBF. If only the bottom 3-meters are measured and results are extrapolated for the entire cross section the estimated CFM would be 819 m^3/s (1,734,000 CFM) and 446 m^3/s (946,000 CFM) respectively, which results in an overestimation of airflow by approximately 448 m^3/s (950,000 CFM ~ 220%) and 42 m^3/s (89,000 CFM ~ 110%) for Fig. 14A and B. Furthermore, Fig. 13D shows a cross section near the exhaust poral and the EF. However, in this instance the airflow is underestimated by the lower 3-meter traverse by approximately 221 m^3/s (470,000 CFM ~ 35%). When non booster fan entries are investigated a more equivalent extrapolation is reached such as Fig. 14C for example. The extrapolated and total CFM values are within ~ 1 m^3/s (1000 CFM) of each other ~ 99% accuracy. Fig. 14 shows vast differences, from 210% to 35%, between the calculated total airflow in the entry and the extrapolated airflow from the bottom 3-meters of the cross section, with the most inaccuracies in the booster fan entries. Additionally, these calculated airflows from the CFD model are modeled results. When mine operators take anemometer measurements, they assume further error from the instrument and the user which will only cause more uncertainty around these measurements. The geometry of the mine will play a significant role in determining airflow distribution so there is no overarching solution for all cases; however, the velocity profile of a given cross-sectional area is complex and more errors seem to be associated with the booster fan entry because large cross-sectional area and booster fan induced air turbulence. Nonetheless, if measuring the full traverse is not possible or too cumbersome for the mine operator, the results indicate that taking airflow in a non-booster fan entry is ideal for extrapolated accuracy. Or if the booster fan entry must be measured a cross section further downwind of the booster fan can dramatically improve accuracy. The large opening mine velocity survey should be properly planned for accurate airflow estimation and the air flow velocity profile should be considered when the extrapolated velocity is being used from the lower portion of the whole opening.

5.2. *Mechanism of pollutant dilution in large opening mine work headings*

Airflow in and around the CFD geometry is driven by the IBF. The high velocity regions of the model (0.5 m/s to 5 + m/s) are shown by Fig. 15A. Near the center of the geometry the airflow is drawn into the IBF from all the entries around it, while downwind of the IBF recirculation occurs on both sides of the IBF entry. However, this recirculation is minimal because only adjacent entries show this recirculation with most other entries showing a grey color which indicates an air velocity bellow 0.5 m/s (98.4 k CFM assuming a 1000 ft^2 cross section). For a better perspective on this lower velocity region, Fig. 15B shows air velocities from 0 m/s to 0.5 m/s. These airflow patterns show airflow is

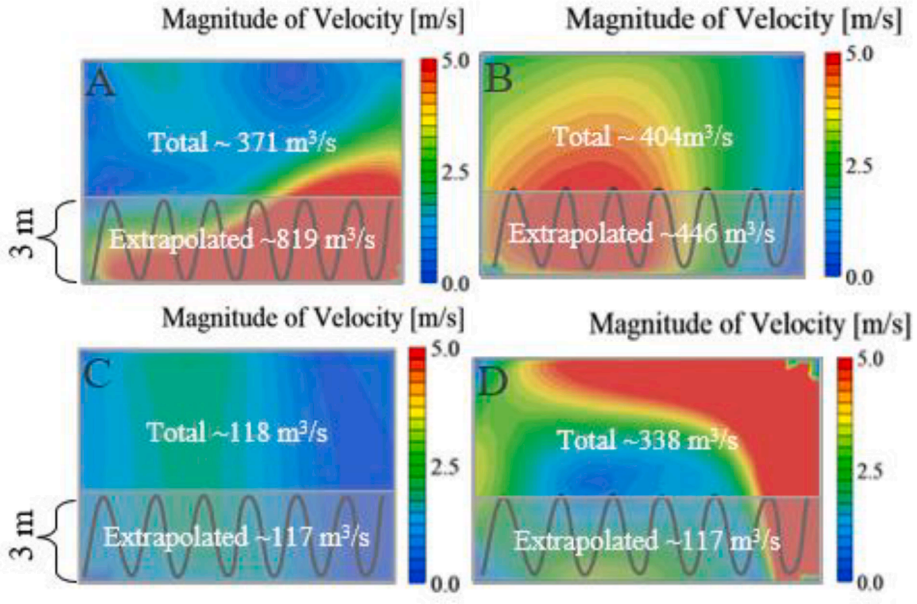

Fig. 14. Magnitude of velocity at four locations and calculated CFM values for both the entire cross section and the extrapolated CFM from a typical continuous traverse (bottom 3-meters): A) 1 pillar outby the IBF (6_N, 7_W-8_W), B) 4 pillars outby the IBF (6_N, 10_W-11_W), C) 3 pillars outby IBF and 1 entry to the west, (5_N, 9_W-10_W), D) 5 m inby Exhaust portal.

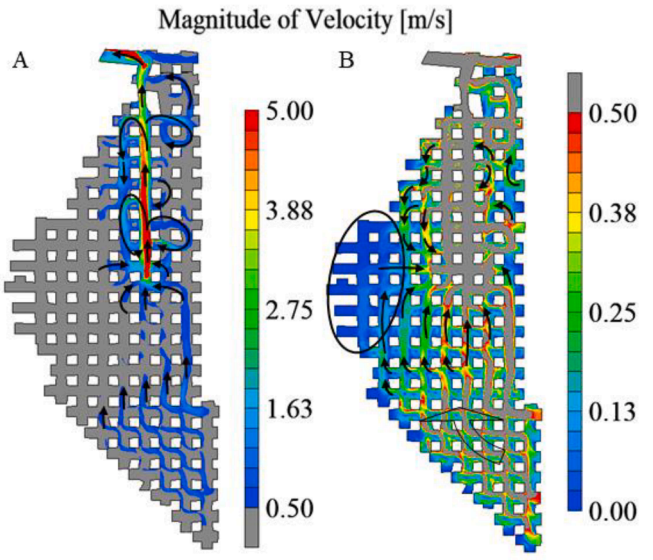

Fig. 15. Velocity contours of CFM model 2 m above the floor separated at high and low velocity levels with black arrows showing the general airflow trend: A) high velocity values 0.5 m/s to 5 + m/s B) low velocity values 0 m/s to 0.5 m/s.

recirculated back towards the face area outby the IBF while the entries directly the left of the IBF are pulled inward towards the IBF. The airflow inby the IBF is distributed between the entries and is slowly swept across the entries to reach the inlet area of the IBF. While the western most entry, shown in the black circle in Fig. 15B, shows little airflow this region would be highly active for machinery and mining activity which would cause localized turbulence and dispersion to the other entries where pollutants it would be more readily carried to the IBF and streamlined out of the mine.

Fig. 15 shows that booster fans can create significant turbulence and mixing within 1–2 adjacent entries with diminishing airflow up to 4–5 entries away from their entry. Indicating that booster fans are an effective airflow control for large opening mines up to 4–5 adjacent entries away from the booster fan entry. This may be adequate for dilution and airflow it may not be optimal for the system, and the question remains on where the optimal booster fan placement is for this section.

6. Summary and conclusion

In this study, we conducted a field survey for the large opening mine and the survey data serve as the numerical modeling inputs to investigate the localized airflow distribution using CFD model. Based on the survey data and modeling results, the following conclusions can be made:

(1) Booster fan is an effective ventilation control for airflow direction in large opening mine and the booster fan placement can significantly influence the effectiveness of face ventilation airflow recirculation.
(2) The velocity profile of a given cross-sectional area is complex due the large opening size and booster fan induced air turbulence. Consideration should be given to not take airflow readings near the booster fans which were shown to over or under estimate airflow by as much as 210% and 35% respectively.
(3) The airflow calculated at the second adjacent entry was 25% of the fan setting with the subsequent entries exchange diminishing by ~ 65.2% per entry.
(4) The geometry of the mine will play a significant role in determining the airflow distributions and attention must be given to understand the recirculation patterns around the booster fans for each specific mining section.

Pressure differential naturally drives airflow, and fans that are typically utilized in these large opening mine settings are low-pressure high-volume fans which naturally makes it difficult to drive airflow in adjacent entries. This study shows the effect that this specific booster fan placement has on the surrounding entries. However, the question remains on how the specific booster fan placement both within the entry and in the overall section will affect its surrounding entries and the face areas.

CRediT authorship contribution statement

Nathan Gendrue: Conceptualization, Methodology, Validation, Formal analysis, Investigation, Writing – original draft, Writing – review & editing, Visualization. **Shimin Liu:** Conceptualization, Methodology, Investigation, Writing – review & editing, Supervision. **Sekhar Bhattacharyya:** Investigation, Funding acquisition. **Ronald Clister:** Investigation.

Declaration of Competing Interest

The authors declare that they have no known competing financial interests or personal relationships that could have appeared to influence the work reported in this paper.

Data availability

Data will be made available on request.

Acknowledgement

This work was financially supported by The National Institute of Occupational Safety and Health (NIOSH) under contract No. 75D30119C05743.

References

Aminossadati, S.M., Hooman, K., 2008. Numerical Simulation of Ventilation Air Flow in Underground Mine Workings. 12th US/North Am. Mine Vent. Symp. 253–260.
Bakker, A., 2021. The colorful fluid mixing gallery [WWW Document]. URL www.bakker.org/index.htm.
Cai, P., Nie, W., Hua, Y., Wei, W., Jin, H., 2018. Diffusion and pollution of multi-source dusts in a fully mechanized coal face. Process Saf. Environ. Prot. 118, 93–105. https://doi.org/10.1016/j.psep.2018.06.011.
Code of Federal Regulations, 2018.
Chang, P., Xu, G., Zhou, F., Mullins, B., Abishek, S., Chalmers, D., 2019. Minimizing DPM pollution in an underground mine by optimizing auxiliary ventilation systems using CFD. Tunn. Undergr. Sp. Technol. 87, 112–121. https://doi.org/10.1016/j.tust.2019.02.014.
Dunn, M.F., Kendorski, F.S., Rahim, M.O., Mukherjee, A., 1983 Testing Jet Fans in Metal/Nonmetal Mines with Large Cross-Sectional Airways, Report for the U.S. Bureau of Mines contract # J0318015.
Grau III, H., Krog, R., 2009. Using mine planning and other techniques to improve ventilation in large-opening mines. Min. Eng. 61, 46–50.
Grau III, R., Mucho, T., Robertson, S., Smith, A., Garcia, F., 2002. Practical techniques to improve the air quality in underground stone mines. Mine Vent. https://doi.org/10.1201/9781439833742.ch19.
Grau III, R.H., Krog, R.B., Robertson, S.B., 2006. Maximizing the ventilation of large-opening mines. Proc. 11th U.S./North Am. Mine Vent. Symp. - 11th U.S./North Am. Mine Vent. Symp. 2006, 53–59. https://doi.org/10.1201/9781439833391.ch8.
Grau III, R. H., Robertson, S.B., Krog, R.B., Chekan, G.J., Mucho, T.P., 2004. Raising the bar of ventilation for large-opening stone mines. Proc. 10th US/North Am. Mine Vent. Symp. 349–355.
Grau III, R.H., Robertson, S.B., Mucho, T.P., Garcia, F., Smtih, A.C., 2004b. NIOSH Ventilation Research Addressing Diesel Emissions and Other Air Quality Issues in Nonmetal Mines. SME Trans. 316, 149–158.
Goodman, G.V.R., Taylor, C.D., Thimons, E.D., 1992. Jet fan ventilation in very deep cuts – a preliminary analysis, US Bureau of Mines Report of Investigations 9399, US Department of the Interior, Pittsburgh, PA, 1992, pp. 1–12.
Hargreaves, D.M., Lowndes, I.S., 2007. The computational modeling of the ventilation flows within a rapid development drivage. Tunn. Undergr. Sp. Technol. 22, 150–160. https://doi.org/10.1016/j.tust.2006.06.002.

Krog, R.B., Grau III, R.H., Mucho, T.P., Robertson, S.B., 2004. Ventilation planning layouts for large opening mines. Soc. Mining, Metall. Explor. 1–9.

Kurnia, J.C., Sasmito, A.P., Mujumdar, A.S., 2014. CFD simulation of methane dispersion and innovative methane management in underground mining faces. Appl. Math. Model. 38, 3467–3484. https://doi.org/10.1016/j.apm.2013.11.067.

Lee, C.W., Nguyen, V.D., 2015. Development of a Low Pressure Auxiliary Fan for Local Large-opening Limestone Mines. Tunn. Undergr. Sp. 25, 543–555. https://doi.org/10.7474/tus.2015.25.6.543.

Mcpherson, M.J., 1993. Subsurface Ventilation Engineering. M. J. McPherson.

Mishra, D.P., Kumar, P., Panigrahi, D.C., 2016. Diffusion and pollution of multi-source of a retreating longwall mine: a computational fluid dynamics study. Environ. Earth Sci. 75 https://doi.org/10.1007/s12665-016-5319-9.

Nguyen, V., Lee, C., 2019. Optimization of the unducted auxiliary ventilation for large-opening underground limestone mines. Tunn. Undergr. Sp. 29, 480–507. https://doi.org/10.7474/TUS.2019.29.6.480.

Nguyen, V.D., Heo, W.H., Kubuya, R., Lee, C.W., 2019. Pressurization ventilation technique for controlling gas leakage and dispersion at backfilled working faces in large-opening underground mines: CFD analysis and experimental tests. Sustain. 11 https://doi.org/10.3390/SU11123313.

Parra, M.T., Villafruela, J.M., Castro, F., Méndez, C., 2006. Numerical and experimental analysis of different ventilation systems in deep mines. Build. Environ. 41, 87–93. https://doi.org/10.1016/j.buildenv.2005.01.002.

Ren, T., Balusu, R., 2005. CFD Modelling of Goaf Gas Migration to Improve the Control of Spontaneous Combustion in Longwalls CFD Modelling of Goaf Gas Migration to Improve the Control of Spontaneous Combustion in Longwalls 259–264.

Ren, T., Wang, Z., Cooper, G., 2014. CFD modelling of ventilation and dust flow behaviour above an underground bin and the design of an innovative dust mitigation system. Tunn. Undergr. Sp. Technol. 41, 241–254. https://doi.org/10.1016/j.tust.2014.01.002.

Sun, J., Zhang, H., Huang, M., Chen, Q., Chen, S., 2018. Reasonable paths of construction ventilation for large-scale underground cavern groups in winter and summer. Sustain. 10 https://doi.org/10.3390/su10103768.

Tanguturi, K., Balusu, R., Bongani, D., 2017. Goaf gas flow modelling in 6KM long longwall panel 31, 1–15.

Thiruvengadam, M., Zheng, Y., Tien, J.C., 2016. DPM simulation in an underground entry: Comparison between particle and species models. Int. J. Min. Sci. Technol. 26, 487–494. https://doi.org/10.1016/j.ijmst.2016.02.018.

Wala, a.M., Jacob, J.D., Brown, J., Huang, G., 2003. New approaches to mine-face ventilation. Mineing Eng. 55, 25–30.

Wang, Z., Ren, T., Ma, L., Zhang, J., 2018. Investigations of ventilation airflow characteristics on a longwall face—a computational approach. Energies 11, 1–25. https://doi.org/10.3390/en11061564.

Xu, G., Luxbacher, K.D., Ragab, S., Xu, J., Ding, X., 2017. Computational fluid dynamics applied to mining engineering: a review. Int. J. Mining. Reclam. Environ. 31, 251–275. https://doi.org/10.1080/17480930.2016.1138570.

Yuan, L., Smith, A., Brune, J., 2006. Computational fluid dynamics study on the ventilation flow paths inlongwall gobs. 11th US/North Am. Mine Vent. Symp. 2006, 591–598. https://doi.org/10.1201/9781439833391.ch83.

Zhai, Z.J., Zhang, Z., Zhang, W., Chen, Q.Y., 2007. Evaluation of various turbulence models in predicting airflow and turbulence in enclosed environments by cfd: Part 1—summary of prevalent turbulence models. HVAC R Res. 13, 853–870. https://doi.org/10.1080/10789669.2007.10391459.

Zhang, X., Zhang, Y., Tien, J.C., 2011. The Efficiency Study of the Push-pull Ventilation System in Underground Mine. 11th Undergr. Coal Oper. Conf. 225–230.

Zheng, Y., Tien, J.C., 2008. DPM Dispersion Study using CFD for Underground Metal / Nonmetal Mines. 12th U.S./North Am. Mine Vent. Symp. 487–494.

Zheng, Y., Li, Y., Thiruvengadam, M., Lan, H., Tien, J.C., 2017. DPM dispersion inside a single straight entry using dynamic mesh model. Int. J. Coal Sci. Technol. 4, 234–244. https://doi.org/10.1007/s40789-017-0179-9.